Revista Brasileira de **Física, Vol. 7, Nº 2, 1977**

Relative Radiative Decay Rates of Vacancies in L-Subshells of Heavy Elements*

C. V. BARROS LEITE, A. G. DE PINHO and N. V. DE CASTRO FARIA
*Departamento de Física, Pontifícia Universidade Católica**, Rio de Janeiro RJ*

Recebido em 11 de Março de 1977

Relative radiative decay rates of vacancies in L-subshells were measured for a large number of heavy elements with a Si(Li) detection system. A graphical method was employed to analyse the x-ray. spectra so obtained. Systematic results are presented together with other already published results obtained in our laboratories in recent years. This covers the interval $74<Z<93$. Results are compared with theoretical predictions and experimental data from other authors, and some general features are noted.

Mediram-se taxas relativas de decaimentos radiativos de lacunas em sub-camadas L , para um grande número de elementos pesados, com um sistema de deteção de Si(Li). Empregou-se um método gráfico para analisar os espectros de raios-x obtidos. Apresentam-se resultados sistemáticos juntamente com outros já conhecidos, também obtidos em nossos laboratórios nos Últimos anos, o que cobre o intervalo $74<Z<93$. Comparam-se os resultados com previsões teóricas, como também com dados experimentais de outros autores, chamando-se atenção sobre certas características gerais.

* Work supported by grants from CNPq and FINEP (Brazil).

** Postal Address; Rua Marquês de São Vicente, 209/263, Rio de Janeiro, RJ.

1. INTRODUCTION

L x-ray spectra arise following the transference of electrons to fill vacancies in the L levels. Since there are three L subshells, compared with only a single K level, there will be a far greater complexity in L spectra than in K spectra, and normally about 15 to 20 lines are observed from the higher atomic number elements with a good resolution Si(Li) detection system. These spectra contain mainly normal (diagram) lines but a few forbidden Ml and E2 transitions are sometimes identified. Moreover, the presence of transitions resulting from other more complicated processes can introduce further difficulties. Satellite lines occur both on the high-energy side and on the low-energy side of the reference lines. In the first case, the satellite lines are due to double vacancy production either by Auger (KLX) or Coster-Kronig (L_iL_jX) transitions or by direct double ionization by charged particle impact. In the second case, the satellite lines are due to radiative Auger transitions. In the case of multiple ionization by direct impact, the intensities of the satellite lines relative to the reference (normal) line are obviously dependent on the creation mechanism of the vacancies (e.g., the charge and the energy of the ionizing particle). The relative importance of satellite lines due to outer vacancies following Auger and Coster-Kronig transitions are also dependent on the primary distribution of vacancies, i.e., on the creation mechanism. On the other hand, an independente of the mechanism of the L-shell vacancy is to be expected in the case of radiative Auger transitions.

The analysis of such complex spectra requires a high resolution detection system. Though Si(Li) detectors are worse in energy resolution than crystal spectrometers, they offer some advantages, specially for measurements at higher x-ray energies, e.g., higher overall detection efficiency, absence of spurious peaks, and simultaneous accumulation of the entire energy spectrum, which results in much better statistics.

During the past severa1 years, a number of experiments have permitted the measurement of the ratios of L-subshell emission rates. Vacancies can be produced by interna1 conversion, by electron capture, or by collisions. The first method was employed in this laboratory[1-4] to measu-

re relative radiative decay rates in TR, Bi, Ra, Rn, Ac and Np. We are now reporting results obtained by ionizing W, Au, Tℓ, Pb, Bi, Th and U atoms, with protons in the energy range from 0.5 to 3.5 MeV. For these energies, multiple ionization by direct impact is shown to be negligi- and so comparison with previous results and with theoretical predicti- ons is possible. These theoretical results are based on the relativis- tic self-consistent Hartree-Fock-Slater potential. Scofield's calcula- tions[5] are for a point nucleus, while Rosner and Bhalla[6] included the effect of finite size of the nucleus. They both include the effect of retardation and their numerical results agree to within three signifi- cant figures. More recently, Scofield[7] improved his result by using separate Hartree-Fock calculations for the initial and final wave func- tions. Assuming a Coulomb potential and relativistic screened wave func- tions, Babushkin[8] calculated the intensity ratios of severa1 K and L x-ray transitions for many elements. Except for the choice of the po- tential, all of these calculations bear close association onetoanother.

Previous systematic measurements, on the L x-ray emission rates of ele- ments with high atomic numbers ($Z>60$), were performed by Victor[9], Goldberg[10] and Salem et $al.$[11,12] with crystal spectrometers. Their re- sults are presented together, graphically, in two recent compilations by Salem[13,14] and will be not reproduced here. As a rule, the expe- rimental points are scattered around the theoretical curves of Scofield, as is illustrated in Fig. 1.

2. EXPERIMENTAL METHOD AND DATA ANALYSIS

In the present experiment, the vacancies were produced by proton impact. The PUC/RJ 4 MeV Van de Graaf accelerator has provided the proton beam for the experiments. Currents were maintained between 30-200 nA to avoid extreme dead time with consequent peak deformation and electronic pile up problems. The target thickness was always kept small ($\sim 50 \mu g/cm^2$), in order to minimize proton energy loss and self absorption of the x- -rays in the target. Both effects were neglected in the following. The targets were prepared by vacuum evaporation of W, TR, Pb, and Bi onto thin Formvar films, and Th and U onto 100 g/cm^2 Aℓ backing foils. The Au

foil was self supporting. The purity of the targets was* better than 99.98% (99.8% for Th and U) according to the manufacturer. Targets were oriented at 45^{o} with respect to the beam. The x-rays were detected by a Si(Li) detector with a measured resolution of 190 eV at 6.4 keV. The detector was positioned outside the target chamber at an angle of 90^{o} to the incident beam direction. The vaccum separation was maintained by a 4mm diameter Mylar window 6 microns thick. A thin Aℓ foil in front of the detector was used to attenuate the strong M x-rays. Although the presence of the absorber eliminates the sum peaks, it also provokes a rounding-off of the continuous background in the L_{ℓ}-L_{α} region, introducing a supplementary difficulty in the analysis of the data. Standard electronic modules were used. Figure 2 shows a typical spectrum obtained at a bombarding energy of 2 MeV. It is well known that the average separation of the L x-ray lines increases with the atomic number. Thus, more precision should be expected in measuring branching ratios for higher Z elements. However, due to crossing in the transition energies some of the more intense lines of the high Z spectra are less well defined than in the spectra of lower Z elements.

Most of the individual lines in the L_{α}, L_{β} and L_{γ} groups are not fully resolved and a peak fitting procedure has to be used to extract accurate values for the intensities of the lines. A graphical stripping method was employed and full energy peak profiles were determined experimentally for different portions of the spectra. These standard peaks were gamma rays, or K_{α} lines of light elements obtained by proton impact and decomposed into their components by an iterative procedure. The low energy tail of the peaks was carefully determined for each interval of approximately 3 keV. The variaton of the FWHM with the photon energy within the limited range of interest was determined from the measured standards and interpolation at any energy value is possible with an uncertainty not greater than 5%.

* Koch-Light Laboratories Ltd, Colnbrook, Bucks, England.

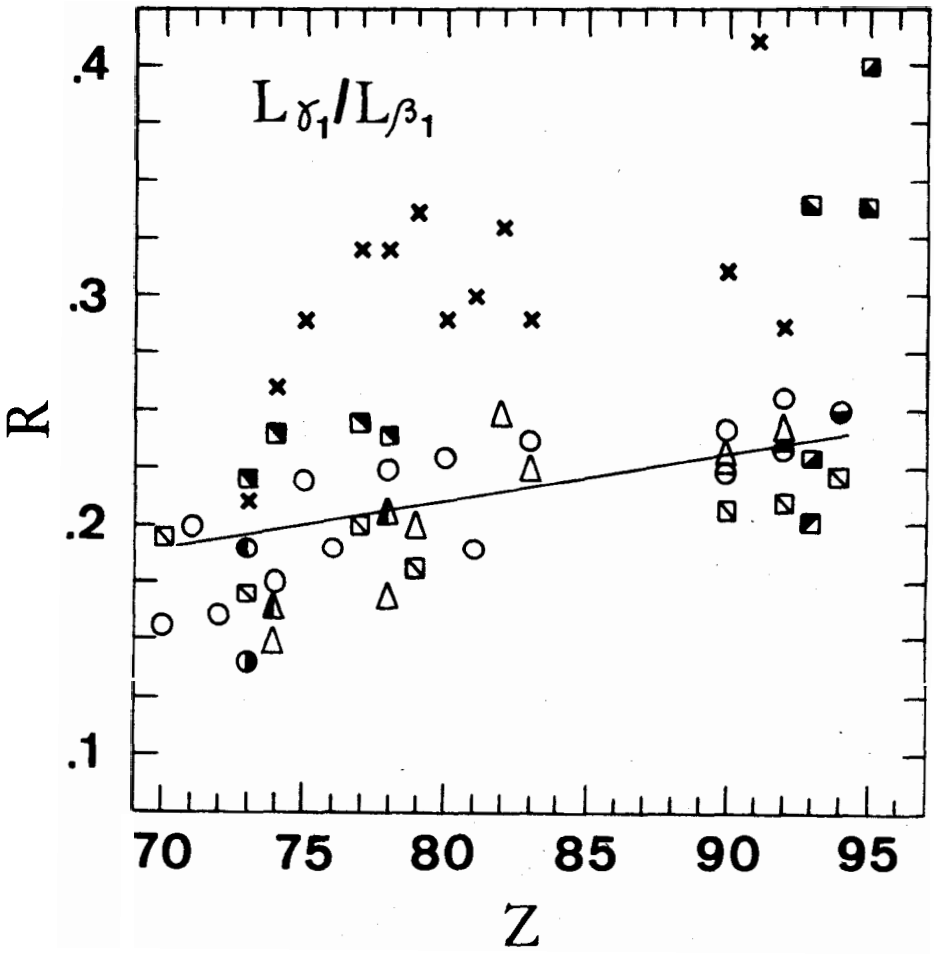

FIG.I. Experimental branching ratio R = L_{γ_1}/L_{β_1} versus atomic number (Z) from Ref. 14. The theoretical curve from Ref.5 is also shown.

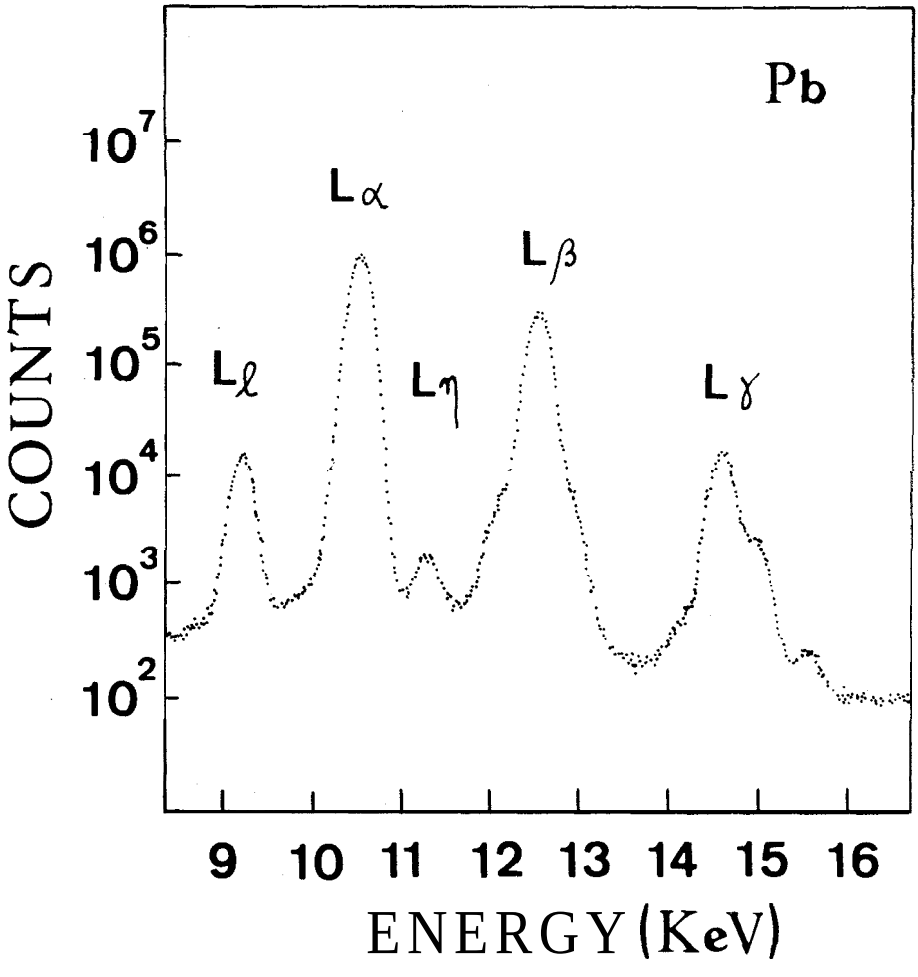

FIG.2. Pb L x-ray spectrum obtained by 2 MeV proton impact.

The presence of auto-ionized satellite lines which are not resolved either from their parent lines or from each other, can introduce a broadening to the high energy side of the lines. This broadening in observed in some L spectra from low Z atoms but is seems unimportant for elements with $Z \geq 70$ when the spectra are recorded with Si(Li) spectrometers. In Refs. 2 and 4, L x-rays following the interna1 conversion of magnetic dipole nuclear transitions were observed, namely the 38.85 keV transition in Tl^{208} and the 46.5 keV transition in Bi^{210}. Since in these cases the number of primary vacancies in the L_{III} subshell is typically of the order of 1 to 2% of the total number of primary vacancies, and since the radiative $L_I L_{III}$ transition is responsible for no more than 4% of the transferred vacancies, almost all the L_α x-rays are emitted in the presence of a second vacancy. However, asymmetries and/or energy shifts of the L_α line were not observed with our semicondutor spectrometer.

Special care was devoted to the determination of the relative efficiency of the x-ray detection system, including the intrinsic efficiency as well as x-ray attenuation by the Mylar window, air path, AR absorber and Be entrance window. K x-rays produced by proton impact on light elements and gamma rays from standard calibrated radioactive sources were employed. The sources were mounted in the chamber at the target location and therefore had a geometry representative of the actual experimental conditions. Background due to the backing foils was considered, but in all cases it was negligible in the energy region of interest.

The errors presented were estimated as the maximum deviation from the average intensity of each peak in various trials of the fitting process. The main sources of errors were the analysis of unresolved peaks and background subtractions. In our graphical stripping method, both operations were performed simultaneously. Peak areas, rather than peak heights, were used in data analysis in order to account for the changes in the peak width. In these conditions, counting statistics introduced negligible error into all the measurements. Corrections to the measured ratios for the overall spectrometer efficiency introduced errors that could be kept less than ± 4%.

3. RESULTS

The values of the L_α/L_ℓ and L_η/L_{γ_1} ratios as a function of proton energy were checked for any variation with energy. Table I lists the slope, in $(MeV)^{-1}$, of a least-squares fitted straight line to the values for L_α/L_ℓ and L_η/L_{γ_1} ratios. The quoted errors were calculated from the experimental errors at each point. No systematic variation of the ratios with the energy was found. This constancy is not surprising since they are branching ratios of transitions to the L_{III} and L_{II} subshells, respectively, and direct multiple ionization is not expected when low energy protons are used for excitation.

On the other hand, the resolution attainable with our spectrometer did not enable the observation of any satellite lines. Although some residual counts were observed in the deepest valleys of the spectra, the origin of these counts was not identified. All experimental results concerning the measured branching ratios are presented in figures 3 to

TABLE 1

Coefficients a (MeV^{-1}) and b, of least squares fitted straight lines $R = aE + b$, for some elements. R is either L_ℓ/L_α or L_1/L_{γ_1}. Values of the proton energies E were taken in the interval 0.5 - 3.0 MeV.

Z	$(L_\ell/L_\alpha) \times 10^2$		$(L_\eta/L_{\gamma_1}) \times 10^2$	
	a	b	a	b
79	-0.21 ± 0.11	5.4 ± 0.3	0.9 ± 0.6	11.6 ± 1.2
81	0.05 ± 0.11	5.4 ± 0.3	0.6 ± 0.6	11.3 ± 1.2
82	0.16 ± 0.10	5.5 ± 0.3	0.4 ± 0.3	10.6 ± 1.2
83	-0.29 ± 0.14	5.8 ± 0.3	-0.5 ± 0.7	12.8 ± 1.4
90	-0.14 ± 0.22	6.6 ± 0.4	-	-
92	0.16 ± 0.17	6.8 ± 0.1	-	-

14. They are compared with the theoretical predictions of Scofield and Babushkin[8] whenever available. Experimental results from other authors[6,17] are also presented for comparison (they were renormalized for convenience, in some cases). In fact, we used the L_{γ_1}, L_{γ_4} and L_α lines as the reference line in the L_I and L_{III} groups, respectively. These lines are well defined in all spectra and are affected only by negligible errors of statistical origin. Thus, the error bars in the branching ratios are essentially due to the errors in the determination of the second transition and the error introduced by relative efficiency of detection (maximum 4% for the most distant pair of transitions as, for instance, L_{β_5}/L_α, L_η/L_{γ_1}, L_η/L_{γ_4}). We observe a very large dispersion among the experimental points even when the error bars are relatively small. Despite this large spread, the experimental data appear tofollow the same general trend exhibited by the theoretical curves. Our results are in closer agreement with Scofield's than with Babushkin's calculations. The most significant discrepancies are observed in the $L_{\gamma_5}/L_{\gamma_1}$ and L_{β_6}/L_α ratios which are systematically larger than theoretical predictions. The behaviour of the "forbidden" $L_{\beta_{9,10}}$ transition is as regular as that of the E1 transitions.

Some special branching ratios are of interest. In Fig. 15, the η/β_1 branching ratio is presented. It is the analog to the γ_5/γ_1 ratio of Fig. 7. Both are $(ns1/2 \rightarrow p1/2) / (nd3/2 \rightarrow p1/2)$ ratios with $n = 3$ and $n = 4$ respectively. They are almost Z-independent, with a tendency to exceed slightly the theoretical predictions. The analog to the R/a ratio (Fig.11) is the $\beta_6/\beta_{2,15}$ ratio (Fig.16); they correspond to $(ns1/2 \rightarrow p3/2)/(nd \rightarrow p3/2)$ ratios with $n = 3$ and $n = 4$, respectively. A gentle increase with Z is observed in both cases. In this region of atomic numbers, the η/β_1 and the γ_5/γ_1 vs Z curves are almost parallel. The theoretical ratio between the curves decreases only 8% from Z = 74 to Z = 93. The same is true for the $\beta_6/\beta_{2,15}$ and the ℓ/α vs Z curves. The absolute value of the ratios (but not their slight Z dependence) can be explained by the dependence of the transition probability on the transition energy.

Another class of interesting branching ratios is that of pairs of transitions with the same initial state of the vacancy and final states with

the same R and j values but differing in the n quantum number as, for instance, the $(4d \rightarrow 2p3/2)/(3d \rightarrow 2p3/2)$ (Fig.12) and $(5d \rightarrow 2p3/2)/(4J \rightarrow 2p3/2)$ (Fig.17) ratios. The theoretical trends predicted by Scofield are very different one from another, and the experimental points agree quite well with the calculations. It is worthwhile observing that the second ratio increases by a factor of 10 in the Z interval considered. The same peculiar behaviour is observed both experimentally and theoretically for the $(4d3/2 \rightarrow 2p1/2)/(3d3/2 \rightarrow 2p1/2)$ (Fig.10) and $(5d3/2 \rightarrow 2p1/2)/(4d3/2 \rightarrow 2p1/2)$ (Fig.8) ratios. The abrupt increase of the second branching ratio with Z is partially related with the increase in the number of electrons in the O shell. The sudden increase of the $\beta_5/\beta_{2,15}$ and γ_6/γ_1 ratios with Z in the region $Z = 74$ to $Z = 90$ is to be compared with the sudden increase of the $\beta_{2,15}/\alpha$ and γ_1/β_1 ratios in the region $Z = 40$ to $Z = 57$, where the N shell is not yet completely filled. When the $4f$ subshell begins to be filled, a change in the slope of the ratios is predicted theoretically and observed experimentally. The same effect is expected to occur when the $5f$ electronic level begins to be filled at $Z = 91$. This situation, noted by Salem[14], is well reproduced by recent calculations of the emission rates in the transuranic elements[18]. A less striking effect is observed in the $(4p \rightarrow 2s1/2)/(3p \rightarrow 2s1/2)$ (Fig.18) and $(5p \rightarrow 2s1/2)/(4p \rightarrow 2s1/2)$ (Fig.5) ratios, but the increase with Z of the branching ratio when the final state is in the O shell is still clearly observed.

Of special interest are the ratios s_1, s_2 and s_3 defined by Rao, Palms and Wood[19] as the ratios of the probability that a vacaricy in the particular L_i subshell ($i = 1,2,3$) will be filled by a radiative transition from a shell above the M shell to the probability that it will be filled by a radiative transition from the M shell. In Fig. 19, the theoretical[17] and experimental results are given for the s_i as a function of atomic number. Whenever the experimental value of the relative transition probability was not attainable, the theoretical rato was recalculated after removing the corresponding theoretical value from the s_i ratio. With the use of separate relativistic Hartree-Fock solutions, an extremely good agreement is reached as in the case of the similar K_β/K_α ratio[20].

CONCLUSIONS

The analysis of the complex L x-ray spectra of higher atomic number elements seems to be the ultimate limit for the present capability of the Si(Li) detectors[15]. Much of the large spread in the experimental data directly reflects the poor resolution of the spectrometer and the intrinsic limitations of the stripping procedure (uncertainties in background subtractionand in ahedeterminationof lineprofiles). Surprisingly enough, the results obtained with the Si(Li) spectrometer are almost as good as those obtained with crystal spectrometers. However, neither method allows clear-cut conclusions about the L x-ray emission rates. The best that can be said is that they seem to follow the general trends predicted by relativistic Hartree-Fock-Slater calculations. Small systematic deviations seem to be firmly established only in a few cases. The possible presence, in the L x-ray spectrum, of fully unresolved satellite lines is a further limitation, of completely unknow extension, in the determination of the intensities of the diagram lines. In fact, the transference of vacancies from the K to the L shell by Auger transitions, and the interna1 redistribution of vacancies among the L subshells by the Coster-Kronig processes, create L-vacancies accompanied by an externa1 second vacancy which modifies both the energy and the transition rates for the radiative filling of the L vacancy. So, even in the absence of direct multiple ionization, and neglecting second order processes, satellite lines are always present but they are undetectable with the usual experimental methods of measuring L branching ratios in the higher Z atoms. On the other hand, the theoretical calculations were not made for radiative transitions in the presence of a second vacancy. The rough agreement between those calculations and branching ratios obtained in widely variable circumstances suggests that the perturbation introduced by these secondary outer vacancies is unimportant. It is however worthwhile observing that with poor resolution spectrometers we are measuring "gross" branching ratios corresponding to the principal plus sattelite lines.

The authors would like to thank Dr. W. R. Owens and G. B. Baptista for reading the manuscript and for helpful comments. The skillful assistance of Mrs. T. Azevedo in the data analysis is kindly acknowledged.

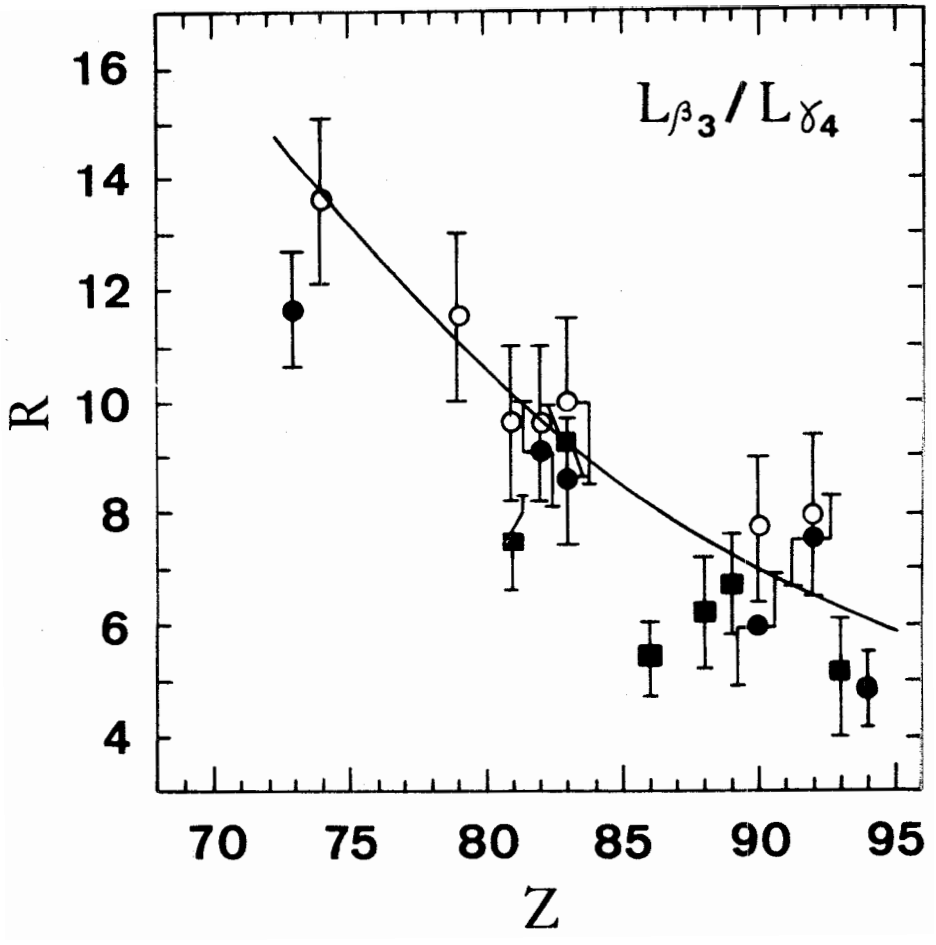

FIG. 3. Experimental branching ratio $R = L_{\beta_3}/L_{\gamma_4}$ versus atomic number (Z). The open circles are our results. The other experimental points are from Ref. 1-4 (squares); Ref. 16 (solid circles). The solid curve is from Ref. 7.

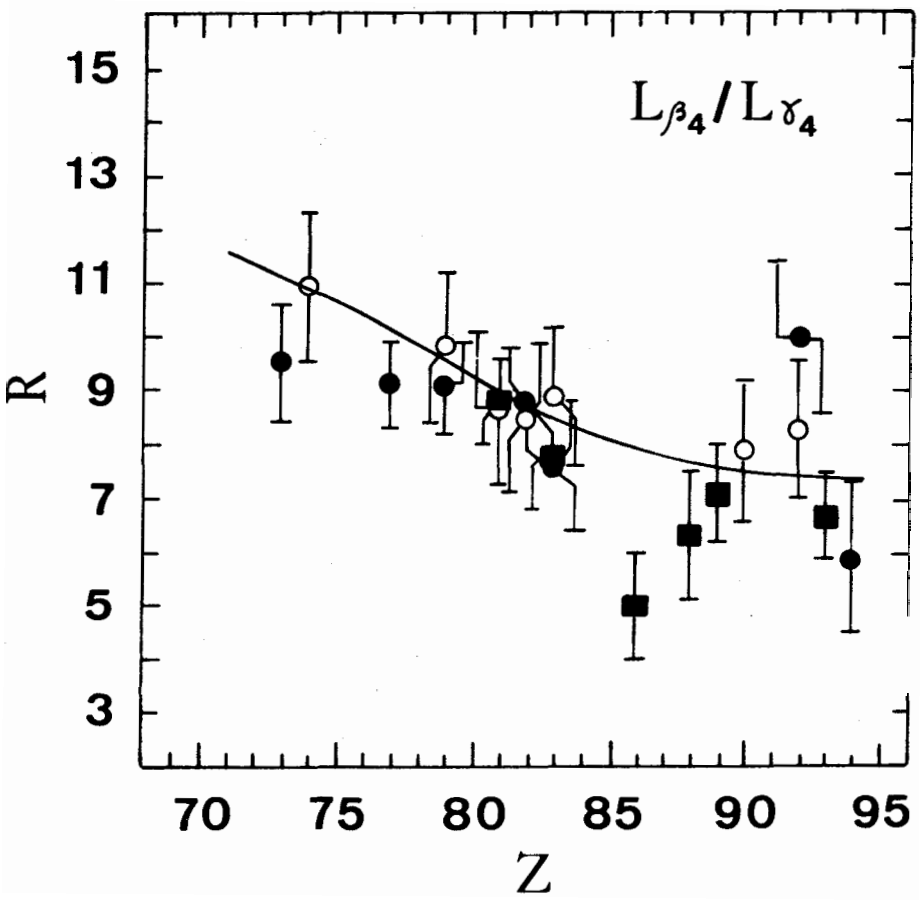

FIG.4. Experimental branching ratio R = L_{β_4}/L_{γ_4} versus atomic number (Z). The open circles are our results. The other experimental points are from Ref. 1-4 (squares); Ref.16 (solid circles). The solid curve is from Ref. 7.

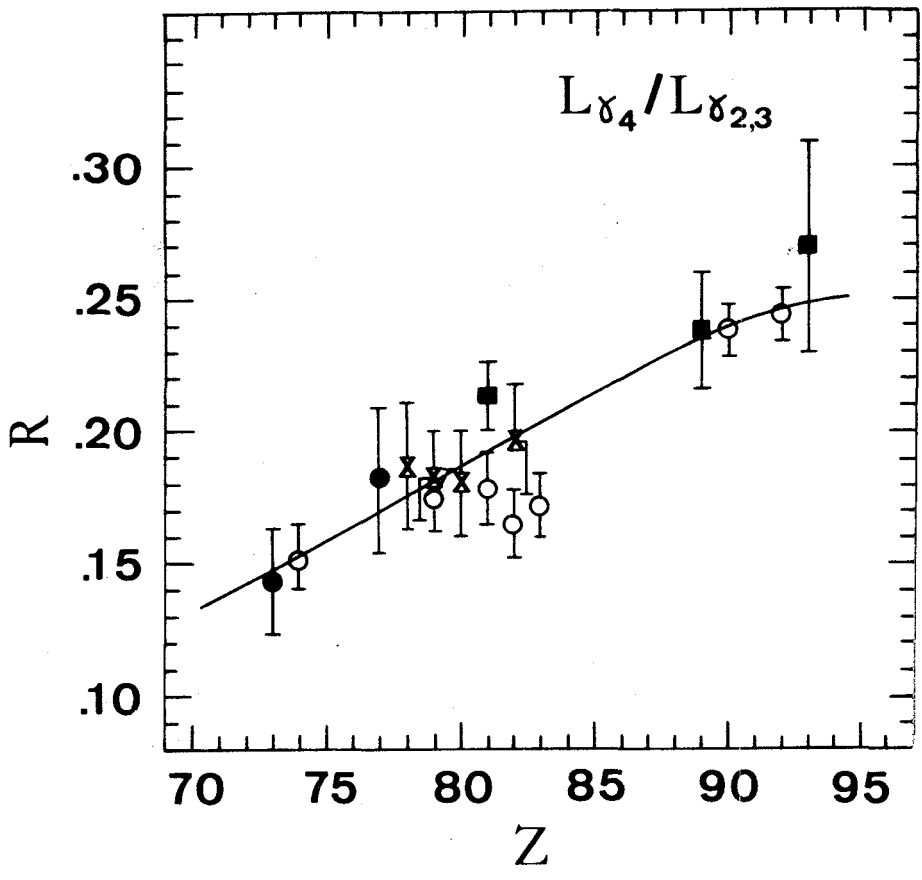

FIG.5. Experimental branching ratio $R=L_{\gamma_4}/L_{\gamma_{2,3}}$ versus atomic number (Z). The open circles are our results. The other experimental points are from Ref. 1-4 (squares); Ref.16 (solid circles) and Ref.17 (crosses). The solid curve is from Ref. 7.

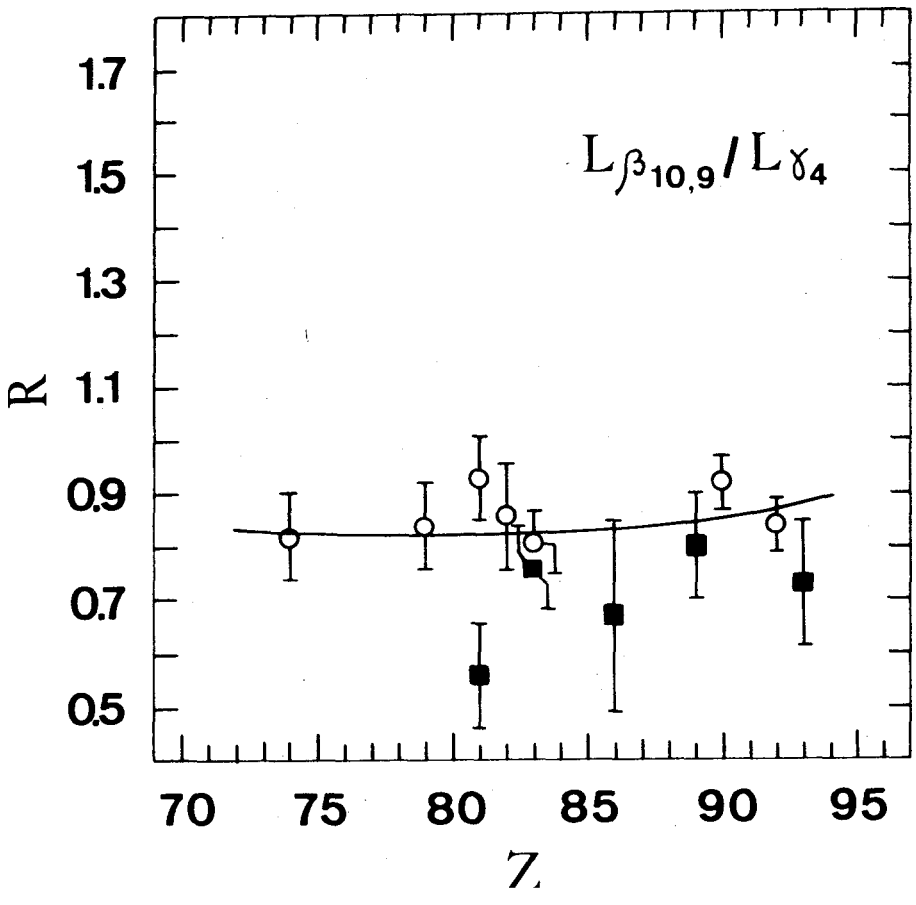

FIG.6. Experimental branching ratio $R=L_{\beta_{10,9}}/L_{\gamma_4}$ versus atomic number (Z). The open circles are our results. The other experimental points are from Ref.1-4 (squares). The solid curve is from Ref. 5.

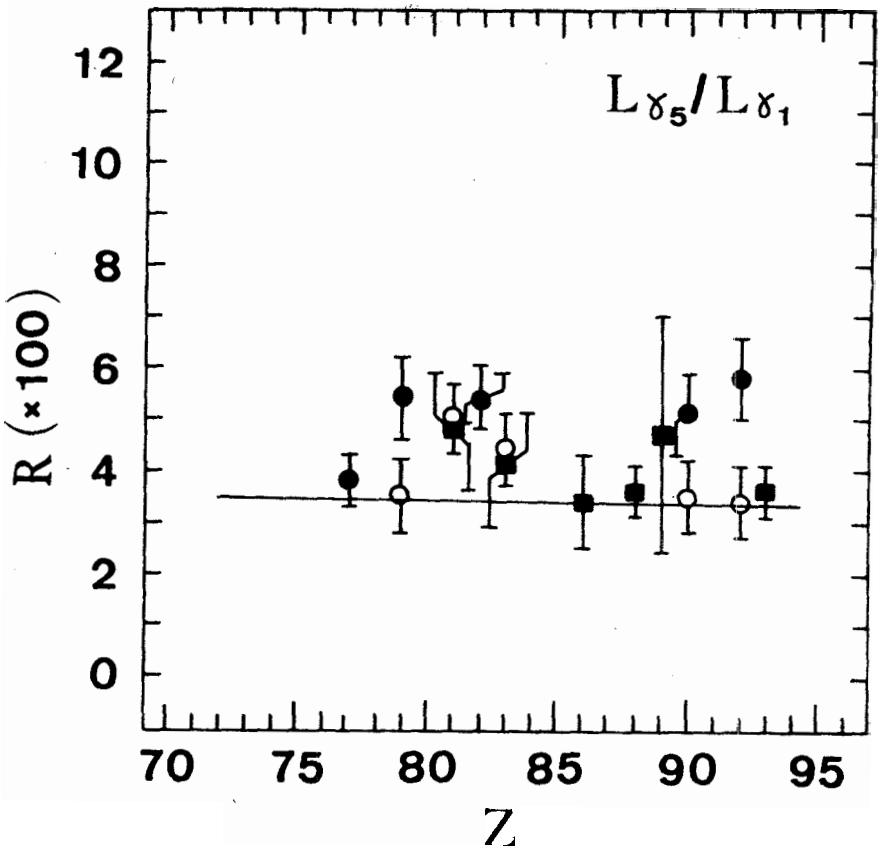

FIG.7. Experimental branching ratio R= $L_{\gamma_5}/L_{\gamma_1}$ versus atomic number (Z). The open circles are our results. The other experimental points are from Ref.[1-4] (squares); Ref.16 (solid circles). The solid curve is from Ref. 7 .

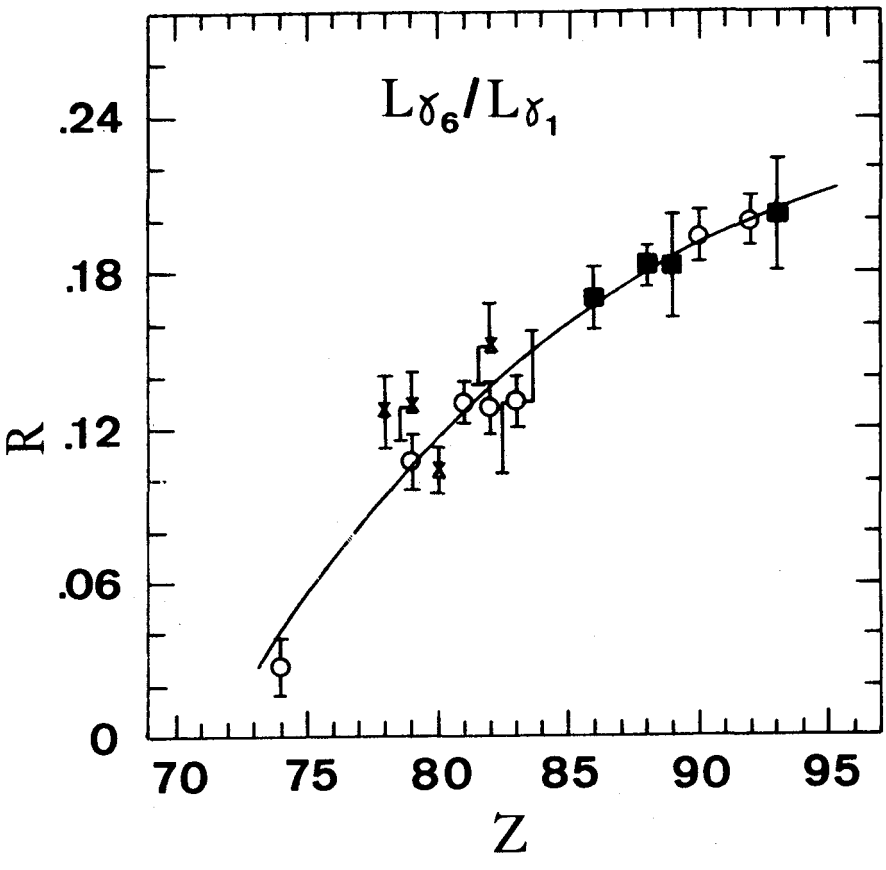

FIG.8. Experimental branching ratio R = $L_{\gamma_6}/L_{\gamma_1}$ versus atomic number (Z). The open circles are our results. The other experimental points are from Ref. 1-4 (squares); Ref. 17 (crosses). The solid curve is from Ref. 7.

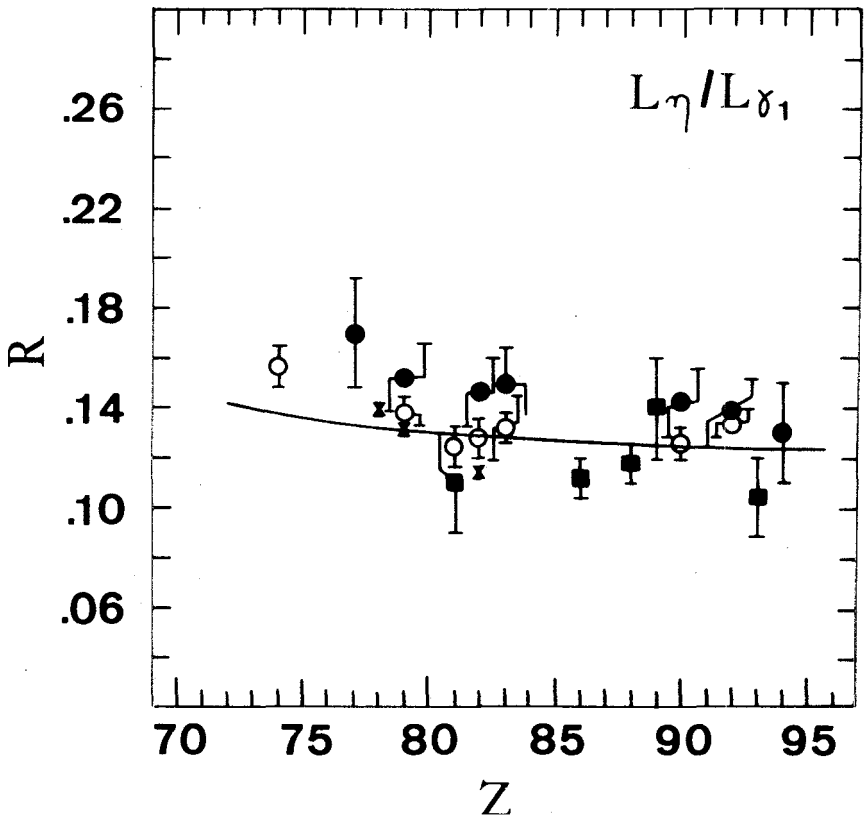

FIG.9. Experimental branching ratio R = L_η / L_{γ_1} versus atomic number (Z). The open circles are our results. The other experimental points are from Ref. 1-4 (squares); Ref.16 (solid circles); Ref. 17 (crosses). The solid curve is from Ref. 7.

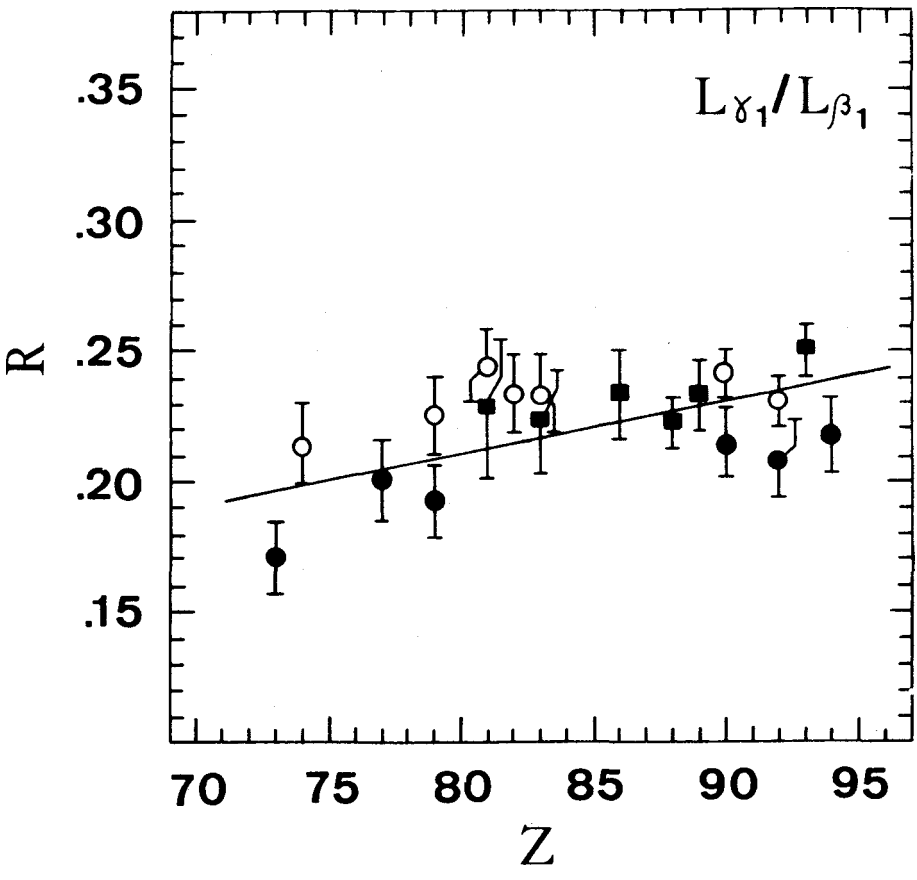

FIG.10. Experimental branching ratio $R=L_{\gamma_1}/L_{\beta_1}$ versus atomic number (Z). The open circles are our results. The other experimental points are from Ref. 1-4 (squares); Ref. 16 (solid circles). The solid curve is from Ref. 7.

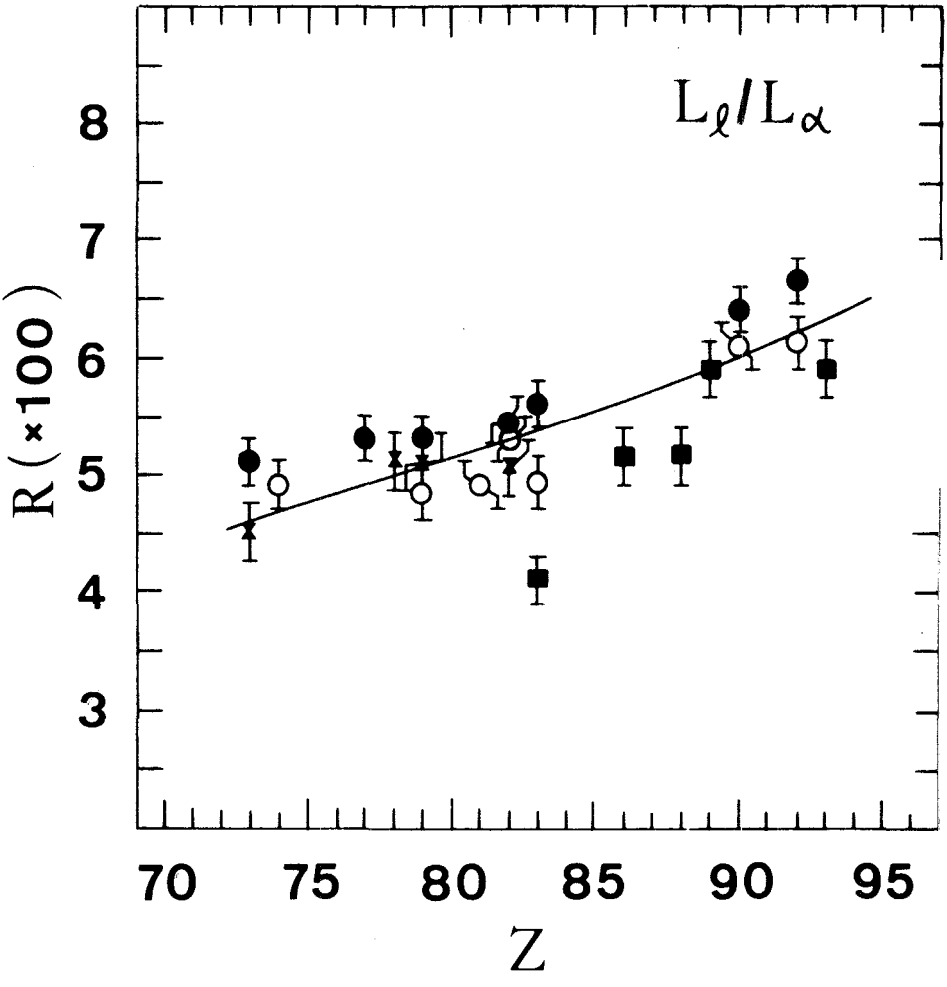

FIG.11.Experimental branching ratio $R = L_R/L_\alpha$ versus atornic number (Z). The open circles are our results. The other experimental points are from Ref.1-4 (squares); Ref.16 (solid circles); Ref.17 (crosses). The solid curve is from Ref. 7.

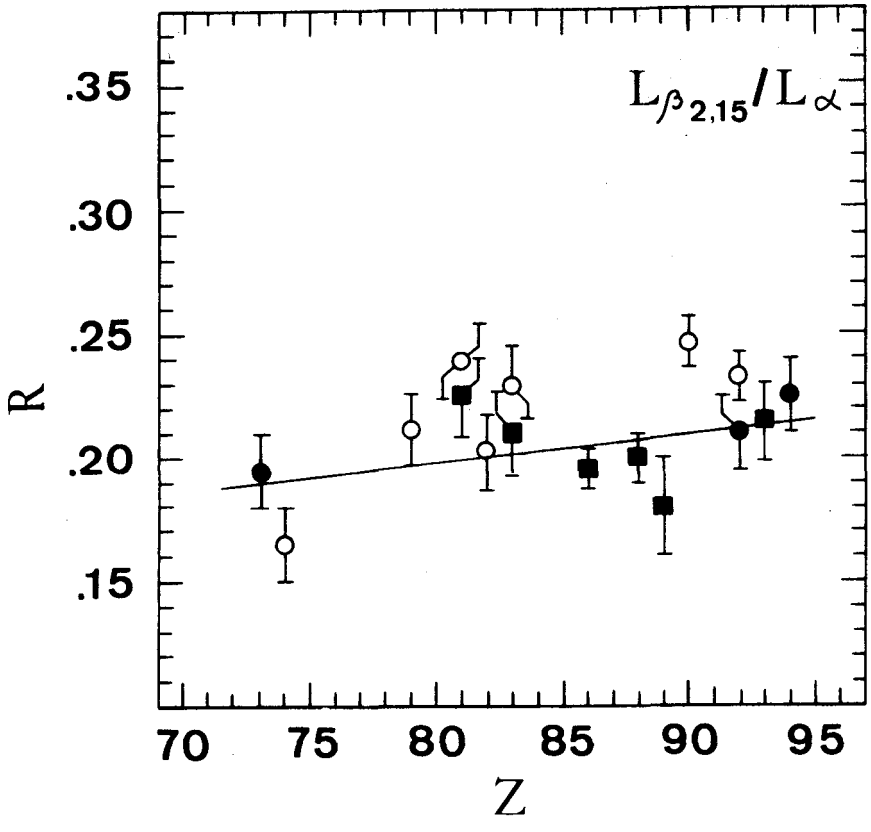

FIG. 12. Experimental branching ratio $R=L_{\beta 2,15}/L_{\alpha}$ versus atomic number (Z). The open circles are our results. The other experimental points are from Ref. 1-4 (squares); Ref. 16 (solid circles). The solid curve is from Ref. 7.

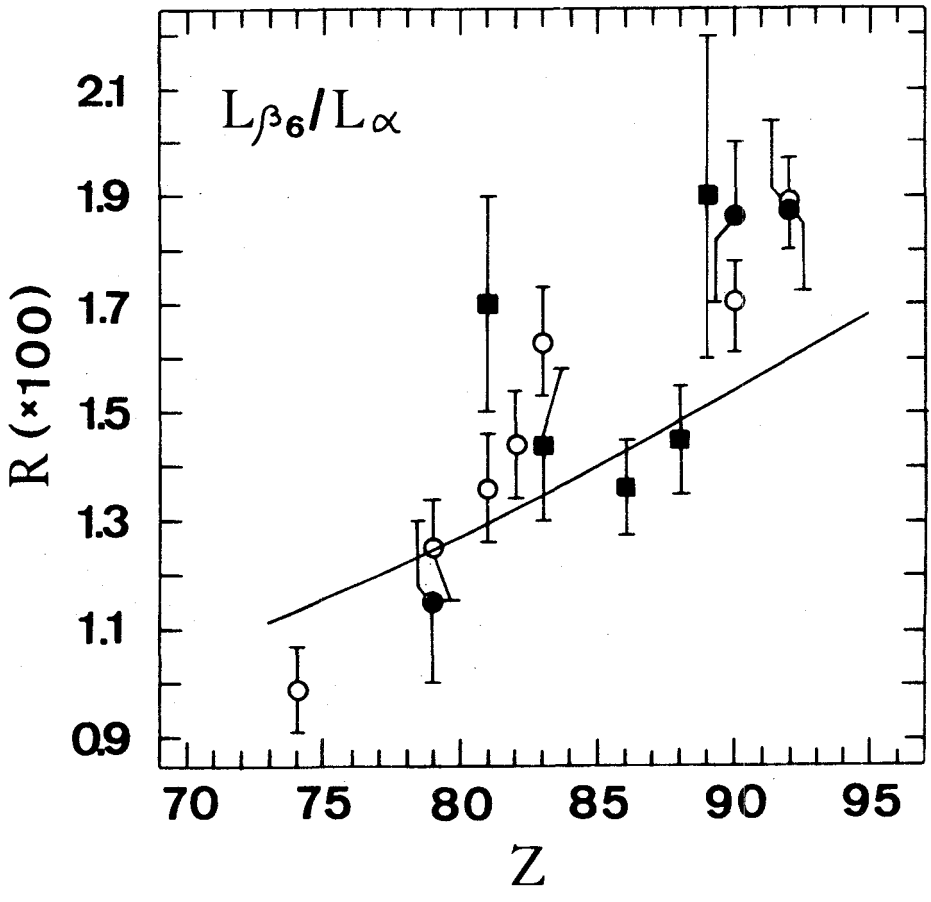

FIG.13. Experimental branching ratio $R = L_{\beta_6}/L_{\alpha}$ versus atomic number (Z). The open circles are our results. The other experimental points are from Ref.1-4 (squares); Ref.16 (solid circles). The solid curve is from Ref. 7.

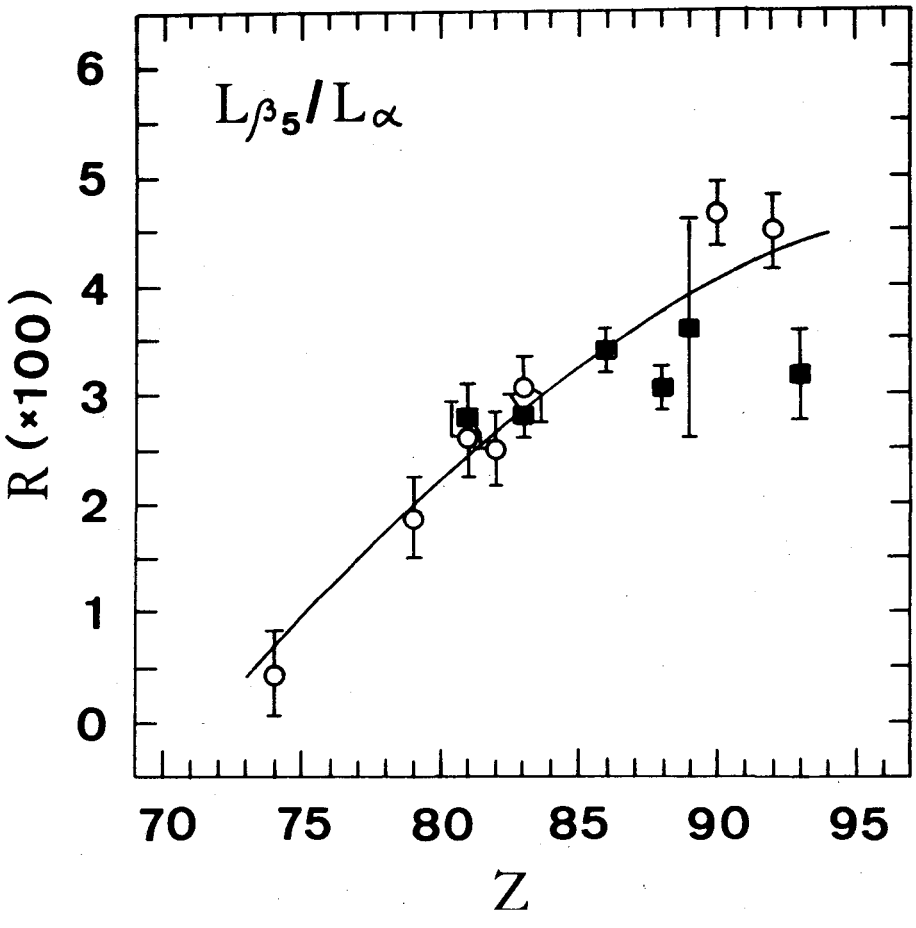

FIG.14. Experimental branching ratio $R = L_{\beta_5}/L_{\alpha}$ versus atomic number (Z). The open circles are our results. The other experimental points are from Ref. 1-4 (squares). The solid curve is from Ref.7.

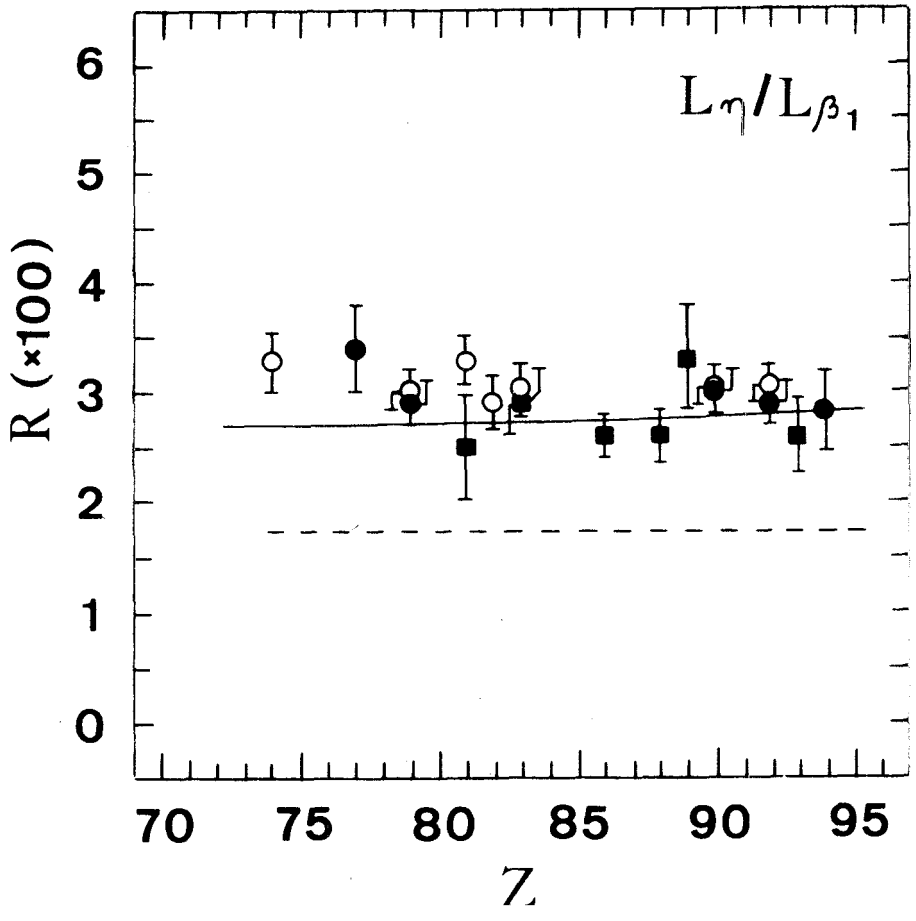

FIG.15. Experimental branching ratio $R = L_{\eta}/L_{\beta_1}$ versus atomic number (Z). The open circles are our results. The other experimental points are from Ref.1-4 (squares); Ref.16 (solid circles). The solid curve is from Ref.7, and the dashed curve from Ref.8.

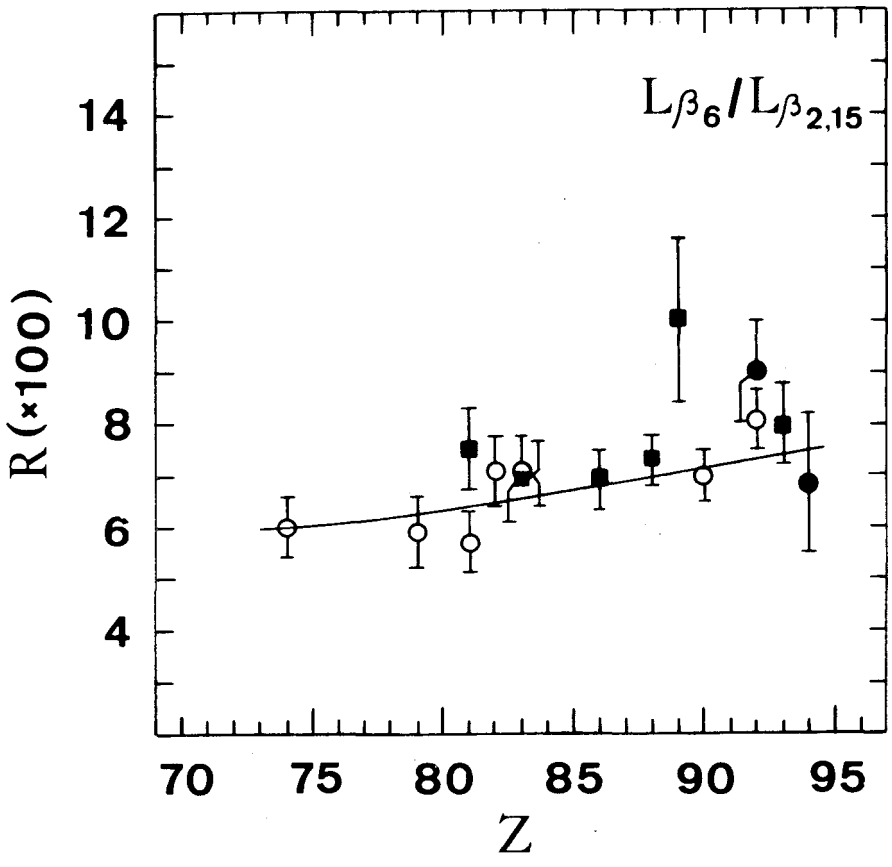

FIG. 16. Experimental branching ratio $R=L_{\beta_6}/L_{\beta_{2,15}}$ versus atomic number (Z). The open circles are our results. The other experimental points are from Ref. 1-4 (squares); Ref. 16 (solid circles). The solid curve is from Ref. 7.

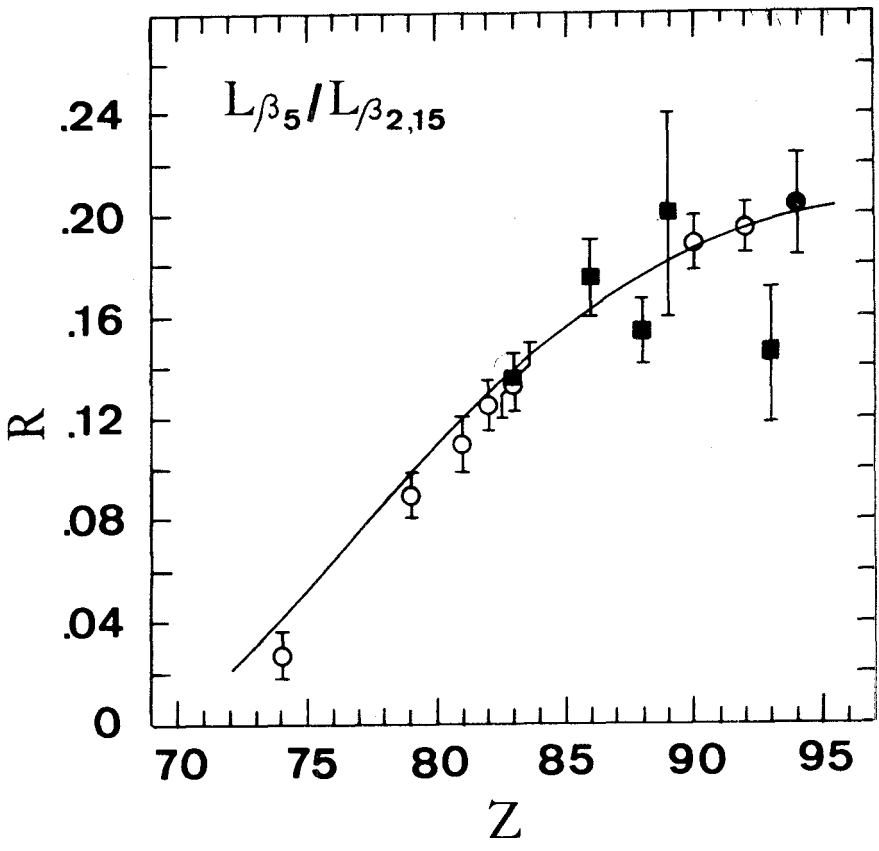

FIG.17. Experimental branching ratio $R=L_{\beta_5}/L_{\beta_{2,15}}$ versus atomic number (Z). The open circles are our results. The other experimental points are from Ref.1-4 (squares); Ref. 16 (solid circles). The solid curve is from Ref.7.

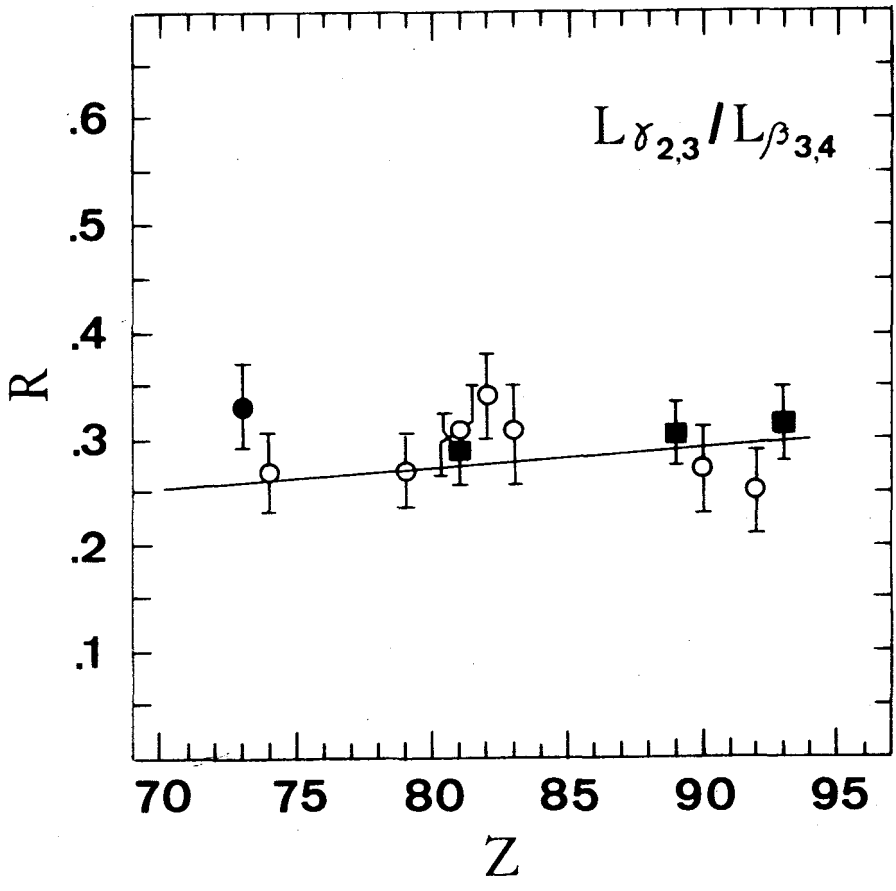

FIG.18. Experimental branching ratio $R=L_{\gamma_{2,3}}/L_{\beta_{3,4}}$ versus atomic number (Z). The open circles are our results. The other experimental points are from Ref.1-4 (squares); Ref.16 (solid circles). The solid curve is from Ref. 7.

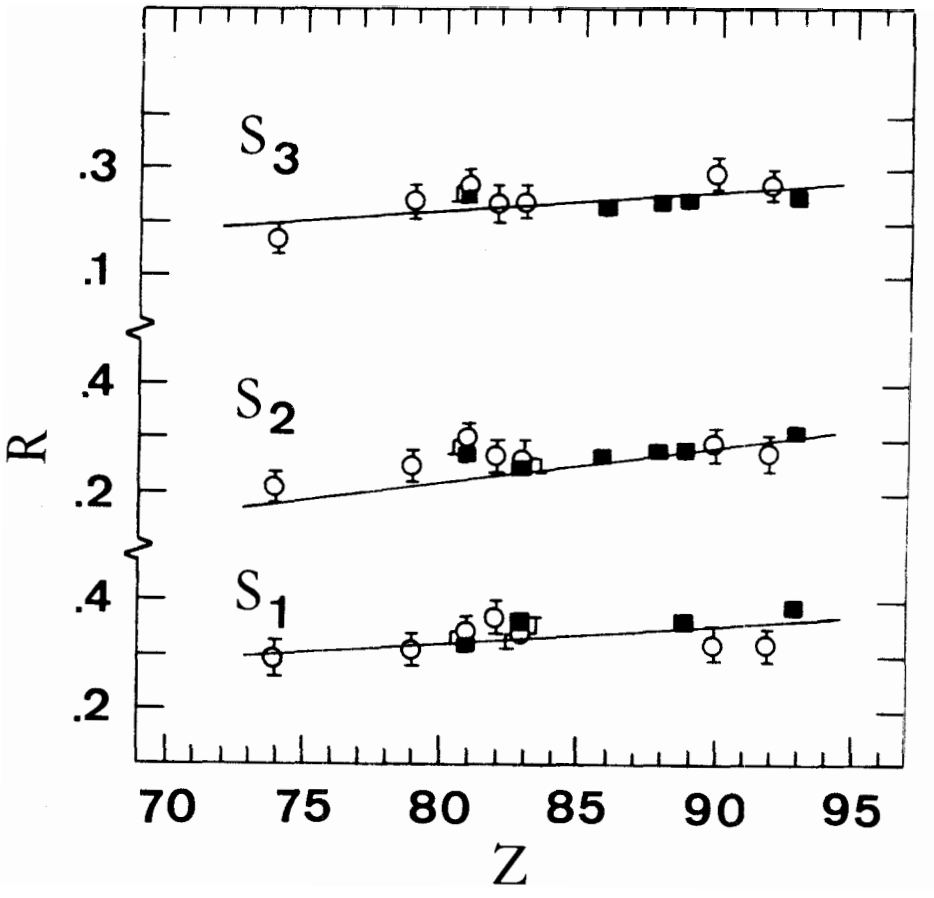

FIG. 19. Theoretical[7] and experimental ratios s_1, s_2 and s_3. Our results are the open circles; the squares are from References 1-4.

REFERENCES

1. A.G. de Pinho and M. Weksler, Z. Naturforsch. *28a*, 1635 (1973).
2. M.Weksler and A.G. de Pinho, Rev. Bras. Fis. 3 291 (1973).
3. A.G. de Pinho, L.T. Auler and A.G. da Silva, Phys.Rev. *C9*, 2056 (1974).
4. L.T. Auler, A.G. da Silva and A.G. de Pinho, Rev.Bras.Fis. *4*, 29 (1974).
5. J.H. Scofield, Phys. Rev. 279, 9 (1969).
6. H.R. Rosner and C.P. Bhalla, Z. Physik 231, 347 (1970).
7. J.H. Scofield, Phys.Rev. *A10*, 1507 (1974), and Phys. Rev. *A12*, 345 (E) (1975).
8. F.A. Babushkin, Opt. i Spectroskopiya, 13, 77 (1962); 13, 141 (1962); 19, 3 (1965) and Acta Phys. Polon. 25, 749 (1964); *31*, 459 (1967); *35*, 883 (1969).
9. C. Victor, Ann. Phys. (Paris) 6 183 (1961).
10. M. Goldberg, Ann. Phys. (Paris) 7 , 329 (1962).
11. S. I.Salem, R.T.Tsutsui and B.A. Rabbani, Phys.Rev. *A4*, 1728 (1971).
12. S.I.Salem, D.C. Clark and R.T.Tsutsui, Phys.Rev. A5, 2390 (1972).
13. S.I.Salem and C.W. Schultz, Atomic Data 3 215 (1971).
14. S.I. Salem, *Proc. Conf. on Inner-Shell Ionization Phenomena*, Atlanta, Ga (USAEC Technical Information Center, Oak Ridge), 1973 (vol.1, pg.285) and Atomic Data *14*, 91 (1974).
15. N.V. de Castro Faria, L.F.S. Coelho, A.G. de Pinho and C.V. de Barros Leite, to be published.
16. J.H. Mc Crary, L.V. Singman, L.H. Ziegler, L.D. Looney, C.M. Edmonds and C.E. Harris, Phys. Rev. *A5*, 1587 (1972).
17. Chen, J.D. Reber, D.J. Ellis and T.E. Miller, Phys. Rev. *A13*, 941, (1976).
18. J.H. Scofield, Atomic Data and Nuclear Data Tables 14, 122 (1974).
19. P.V. Rao, J.M. Palms and R.E. Wood, Phys. Rev. A3, 1568 (1971).
20. J.H. Scofield, Phys. Rev. *A9*, 1041 (1974).